APPROXIMATIONS BY REDUCED-ORDER MODELS FOR NONLINEAR FLUTTER OF VARIABLE STIFFNESS COMPOSITE PLATES

Hamed Akhavan, Pedro Ribeiro

DEMec/INEGI, Faculdade de Engenharia, Universidade do Porto
Rua Dr. Roberto Frias
Porto 4200-465/ Portugal

ABSTRACT

In this investigation, we analyze errors due to using reduced-order models instead of full-order models in the examination of nonlinear flutter of variable stiffness composite laminates (VSCLs). These plates can be made, e.g., by Automated Tow Placement Machines, using composite laminates with curvilinear fibers; in our particular case, the orientation angle of the reference curvilinear fiber path changes linearly from T_0 at the left edge to T_1 at the right edge of the plate. A Third-order Shear Deformation Theory (TSDT) is used to model the laminate and a p-version finite element is applied to discretize the displacements and rotations. The plates are subjected to a supersonic airflow of which the aerodynamic pressure is approximated using linear Piston theory. The equations of motion of the full-order model of the self-excited vibrational system are formed using the principle of virtual displacements. In order to reduce the number of degrees-of-freedom of the full-order model, static condensation and/or a modal summation method are used. The equations of motion of the reduced-order and full-order models are solved using Newmark method to study the dynamic responses, focusing on limit cycle oscillations (LCOs). Approximation errors are discussed for LCO amplitudes of VSCL plates with various curvilinear fiber paths.

1. INTRODUCTION

After a small perturbation, oscillations of a plate subjected to a supersonic airflow with an aerodynamic pressure below a critical value (i.e., below the linear flutter pressure) become stable and static. The linear flutter pressure can be calculated using a linear (small amplitude) structure model associated with a linear aerodynamic model. If the aerodynamic pressure is greater than the linear flutter pressure, oscillations become unstable and a linear analysis predicts that their amplitude grows exponentially. However, geometrical non-linearity, coming from coupling between out-of-plane bending and in-plane stretching of the plate, bounds the oscillation amplitude into a limit cycle oscillation (LCO) [1].

A full-order finite element (FE) model (from now on named as full-model or FOM), including all the physical degrees of freedom (DOFs), predicts the non-linear flutter of a plate without approximations other than the ones ensuing from the theoretical hypothesis on which the model is based upon. However, the solution of full-models with many degrees of freedom entails a large computational cost. In order to reduce this cost, reduced-order models (ROMs) are

SAMPE Conference Proceedings. Charlotte, NC, May 20-23, 2019. Society for the Advancement of Material and Process Engineering – North America.

DOI: *https://doi.org/10.33599/nasampe/s.19.1499*

introduced and, very often, researchers used a limited number of DOFs - generally six to eight [2–9] - in the analysis of nonlinear flutter of plates. The main goal of this study is quantifying the degree of approximation of ROMs with respect to its associated FOM, in plates subjected to supersonic airflow. In this investigation, the order of FOMs will be reduced using static condensation, or by transferring to a reduced number of modal coordinates, or by both procedures.

Mostly classical plate/laminate theory (CPT/CLT) or first-order shear deformation theory (FSDT) have been adopted in the literature. In the current research, the authors use a third-order shear deformation theory (TSDT) to include the effect of thickness to length ratio; TSDT leads to more accurate stress computation than lower order theories and, particularly on thicker plates, also to more accurate computation of deflections.

To carry out the numerical tests, an in-house Fortran code that was developed and validated in the past by the authors is now updated to find the nonlinear flutter response of variable stiffness composite laminated (VSCL) plates. The mentioned code has been validated and used for the analysis of linear vibration [10], static deflection [11], stresses and failure [12], free and forced non-linear vibrations with or without initial imperfections [13–18], and, finally, for the analysis of linear flutter [19]. In the current paper, Newmark method is used for finding the solution for four developed models, listed as:

1) FOM: full-order system with physical DOFs (DOFs from *p*-version finite element);

2) ROM1: reduced-order system with the application of static condensation;

3) ROM2: reduced-order system in modal coordinates, using linear structural modes of FOM;

4) ROM3: reduced-order system, which is first statically condensed and then transferred into modal coordinates, using linear structural modes of ROM1;

In order to apply the analysis on an advanced material with applications in aerospace industry, composite plates with curvilinear fibers (as one type of VSCLs [20]) are evaluated in this investigation. These laminates can be made, for example, by an Automated Fiber Placement machine [21]. This concept of curvilinear fibers allows re-distribution of stresses from high-stress locations in a panel to other stiffer areas. As example of its application, curved fiber paths around a hole in a plate or around windows in an airplane fuselage can avoid stress concentrations [22].

In recent years, some researchers have investigated on linear flutter of VSCLs where curvilinear fiber orientation angles change [23-26]. In what concerns nonlinear flutter of VSCLs, the effect of curvilinear fiber orientation angles is not studied yet. Therefore, the authors believe that this study is helpful for researchers who want to use ROMs in nonlinear flutter analyses of VSCLs. The current paper complements another investigation by the authors [27] where the degree of approximation of ROMs with respect to the associated FOM was studied in thick and imperfect VSCLs and when viscous damping was present. Furthermore, although this study specifically targets VSCLs with curvilinear fibers, its conclusions are of interest to plates on other materials.

2. EQUATIONS OF MOTION OF NONLINEAR FLUTTER OF VSCLS

A rectangular laminate (represented in Figure 1) and a Cartesian coordinate system (x,y), with its origin located in the geometric center of the undeformed plate, are considered. The laminate is symmetric about its middle plane, with length, width, and thickness equal to a, b, and h, respectively. The reference fiber path in any ply of the laminate is curvilinear and its angle $\theta(x)$ is changing linearly with respect to the x axis according to $\theta(x) = (T_1 - T_0)\,(x + a/2)/a + T_0$. The orientation in the reference fiber path changes linearly from T_0 at the left edge to T_1 at the right edge of any ply in the laminate, where each ply has its own characteristic fiber angles $\langle T_0, T_1 \rangle$. The other fiber paths on the same layer are defined by shifting the reference fiber path in y-direction.

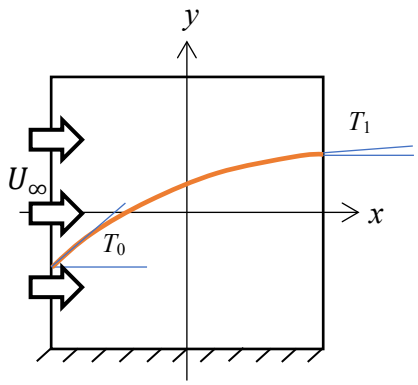

Figure 1. Geometry of a cantilever VSCL plate with a reference fiber path.

A third-order shear deformation theory [28,29] is assumed to define the displacement field,

$$\begin{aligned} u(x,y,z,t) &= u^0(x,y,t) + z\phi_x(x,y,t) - \frac{4z^3}{3h^2}\left(\phi_x(x,y,t) + \frac{\partial w^0(x,y,t)}{\partial x}\right), \\ v(x,y,z,t) &= v^0(x,y,t) + z\phi_y(x,y,t) - \frac{4z^3}{3h^2}\left(\phi_y(x,y,t) + \frac{\partial w^0(x,y,t)}{\partial y}\right), \\ w(x,y,z,t) &= w^0(x,y,t). \end{aligned} \qquad [1]$$

A p-version finite element [30] is used to discretize the mid-plane displacements and rotations as:

$$\begin{Bmatrix} u^0(x,y,t) \\ v^0(x,y,t) \\ w^0(x,y,t) \\ \phi_x(x,y,t) \\ \phi_y(x,y,t) \end{Bmatrix}$$

$$= \begin{bmatrix} \mathbf{N^u}(x,y)^T & \mathbf{0} & \mathbf{0} & \mathbf{0} & \mathbf{0} \\ \mathbf{0} & \mathbf{N^u}(x,y)^T & \mathbf{0} & \mathbf{0} & \mathbf{0} \\ \mathbf{0} & \mathbf{0} & \mathbf{N^w}(x,y)^T & \mathbf{0} & \mathbf{0} \\ \mathbf{0} & \mathbf{0} & \mathbf{0} & \mathbf{N^{\phi_x}}(x,y)^T & \mathbf{0} \\ \mathbf{0} & \mathbf{0} & \mathbf{0} & \mathbf{0} & \mathbf{N^{\phi_y}}(x,y)^T \end{bmatrix} \begin{Bmatrix} \mathbf{q_u}(t) \\ \mathbf{q_v}(t) \\ \mathbf{q_w}(t) \\ \mathbf{q_{\phi_x}}(t) \\ \mathbf{q_{\phi_y}}(t) \end{Bmatrix} \quad [2]$$

The stress-strain relation in an orthotropic lamina is valid in each arbitrary point of any ply made of curvilinear fibers [31]. This relation can be transformed to global coordinates (x and y in Figure 1) using a transformation matrix [31]. A strain-displacement relation retaining von Kármán non-linear terms is considered in this study. Air is considered to flow on the top surface of the VSCL and constant pressure equal to the undisturbed air pressure is set at the lower surface. The pressure difference between the top and the lower surfaces of the plate due to an unsteady supersonic flow, in x direction, can be written using linear Piston theory [32] as

$$\Delta P(x,y,t) = -\frac{2q}{\beta}\left(\frac{M^2-2}{M^2-1}w_{,t}(x,y,t) + w_{,x}(x,y,t)\right) \quad [3]$$

in which a comma before x or t means partial derivative with respect to that parameter. Other parameters on equation [3] are $q = \frac{\rho_\infty U_\infty^2}{2}$ as dynamic pressure; $\beta = \sqrt{(M^2-1)}$; ρ_∞ as ambient density of air; U_∞ as free-stream velocity, and M as Mach number. Based on virtual works of inertia, internal and external aerodynamic forces and using the principle of virtual displacements, the equations of motion of self-excitation vibration (in full order) are in the form of

$$
\begin{bmatrix} \mathbf{M}^{11} & \mathbf{0} & \mathbf{0} & \mathbf{0} & \mathbf{0} \\ & \mathbf{M}^{22} & \mathbf{0} & \mathbf{0} & \mathbf{0} \\ & & \mathbf{M}^{33} & \mathbf{M}^{34} & \mathbf{M}^{35} \\ & & & \mathbf{M}^{44} & \mathbf{0} \\ sym & & & & \mathbf{M}^{55} \end{bmatrix} \begin{Bmatrix} \ddot{\mathbf{q}}_u(t) \\ \ddot{\mathbf{q}}_v(t) \\ \ddot{\mathbf{q}}_w(t) \\ \ddot{\mathbf{q}}_{\phi_x}(t) \\ \ddot{\mathbf{q}}_{\phi_y}(t) \end{Bmatrix}
$$

$$
+ \begin{bmatrix} \mathbf{0} & \mathbf{0} & \mathbf{0} & \mathbf{0} & \mathbf{0} \\ & \mathbf{0} & \mathbf{0} & \mathbf{0} & \mathbf{0} \\ & & \mathbf{F}^{33}_{unsteady} & \mathbf{0} & \mathbf{0} \\ & & & \mathbf{0} & \mathbf{0} \\ sym & & & & \mathbf{0} \end{bmatrix} \begin{Bmatrix} \dot{\mathbf{q}}_u(t) \\ \dot{\mathbf{q}}_v(t) \\ \dot{\mathbf{q}}_w(t) \\ \dot{\mathbf{q}}_{\phi_x}(t) \\ \dot{\mathbf{q}}_{\phi_y}(t) \end{Bmatrix}
$$

$$
+ \left(\begin{bmatrix} \mathbf{K}_{\mathbf{L}}^{11} & \mathbf{K}_{\mathbf{L}}^{12} & \mathbf{K}_{\mathbf{L}}^{13} & \mathbf{0} & \mathbf{0} \\ & \mathbf{K}_{\mathbf{L}}^{22} & \mathbf{K}_{\mathbf{L}}^{23} & \mathbf{0} & \mathbf{0} \\ & & \mathbf{K}_{\mathbf{L}}^{33} & \mathbf{K}_{\mathbf{L}}^{34} & \mathbf{K}_{\mathbf{L}}^{35} \\ & & & \mathbf{K}_{\mathbf{L}}^{44} & \mathbf{K}_{\mathbf{L}}^{45} \\ sym & & & & \mathbf{K}_{\mathbf{L}}^{55} \end{bmatrix} \right.
$$

$$
+ \begin{bmatrix} \mathbf{0} & \mathbf{0} & \mathbf{K}_{\mathbf{NL}}^{13}(\mathbf{q_w}(t)) & \mathbf{0} & \mathbf{0} \\ \mathbf{0} & \mathbf{0} & \mathbf{K}_{\mathbf{NL}}^{23}(\mathbf{q_w}(t)) & \mathbf{0} & \mathbf{0} \\ \mathbf{K}_{\mathbf{NL}}^{31}(\mathbf{q_w}(t)) & \mathbf{K}_{\mathbf{NL}}^{32}(\mathbf{q_w}(t)) & \mathbf{K}_{\mathbf{NL}}^{33}(\mathbf{q_w}(t)) & \mathbf{0} & \mathbf{0} \\ \mathbf{0} & \mathbf{0} & \mathbf{0} & \mathbf{0} & \mathbf{0} \\ \mathbf{0} & \mathbf{0} & \mathbf{0} & \mathbf{0} & \mathbf{0} \end{bmatrix}
$$

$$
\left. + \begin{bmatrix} \mathbf{0} & \mathbf{0} & \mathbf{0} & \mathbf{0} & \mathbf{0} \\ & \mathbf{0} & \mathbf{0} & \mathbf{0} & \mathbf{0} \\ & & \mathbf{F}^{33}_{steady} & \mathbf{0} & \mathbf{0} \\ & & & \mathbf{0} & \mathbf{0} \\ sym & & & & \mathbf{0} \end{bmatrix} \right) \begin{Bmatrix} \mathbf{q}_u(t) \\ \mathbf{q}_v(t) \\ \mathbf{q}_w(t) \\ \mathbf{q}_{\phi_x}(t) \\ \mathbf{q}_{\phi_y}(t) \end{Bmatrix} = \begin{Bmatrix} \mathbf{0} \\ \mathbf{0} \\ \mathbf{0} \\ \mathbf{0} \\ \mathbf{0} \end{Bmatrix} \qquad [4]
$$

Mass, linear and non-linear stiffness sub-matrices, $\mathbf{M}$, $\mathbf{K_L}$ and $\mathbf{K_{NL}}$, are given, for instance, in Ref. [31]. The expressions of the submatrices due to aerodynamic loading are

$$
\mathbf{F}^{33}_{steady} = \frac{2q}{\beta} \int_{\Omega} \mathbf{N}^{w} \mathbf{N}^{wT}_{,x} \, d\Omega
$$

$$
\mathbf{F}^{33}_{unsteady} = \frac{2q}{\beta} \frac{M^2 - 2}{M^2 - 1} \frac{1}{U_\infty} \int_{\Omega} \mathbf{N}^{w} \mathbf{N}^{wT} \, d\Omega \qquad [5]
$$

In an abridged form, the equations of motion of a plate under the action of supersonic flow are

$$
\mathbf{M}\ddot{\mathbf{q}}(t) + \mathbf{F}_{unsteady}\dot{\mathbf{q}}(t) + \left(\mathbf{K_L} + \mathbf{K_{NL}} + \mathbf{F}_{steady}\right)\mathbf{q}(t) = \mathbf{0} \qquad [6]
$$

2.1 Full-Order Model (FOM)

After some convergence tests, it was decided to use seven one-dimensional shape functions in x and y coordinates (leading to 49 two-dimensional shape functions in $\mathbf{N^i}(x,y)^T$) for the discretization of each variable in Equation [2]. The resulting FOM is a system of 5×72=245 equations (DOFs).

2.2 Reduced-Order Model using Static Condensation (ROM1)

Static condensation [33] is useful when in-plane inertia is not noticeable. Putting the in-plane inertia equal to zero, one obtains the in-plane generalized coordinates as a function of the out-of-plane coordinates (from Equation [4]). The resulting equations of motion are

$$\begin{bmatrix} \mathbf{M}^{33} & \mathbf{M}^{34} & \mathbf{M}^{35} \\ & \mathbf{M}^{44} & \mathbf{0} \\ sym & & \mathbf{M}^{55} \end{bmatrix} \begin{Bmatrix} \ddot{\mathbf{q}}_{\mathbf{w}}(t) \\ \ddot{\mathbf{q}}_{\boldsymbol{\phi}_\mathbf{x}}(t) \\ \ddot{\mathbf{q}}_{\boldsymbol{\phi}_\mathbf{y}}(t) \end{Bmatrix} + \begin{bmatrix} \mathbf{F}^{33}_{unsteady} & \mathbf{0} & \mathbf{0} \\ & \mathbf{0} & \mathbf{0} \\ sym & & \mathbf{0} \end{bmatrix} \begin{Bmatrix} \dot{\mathbf{q}}_{\mathbf{w}}(t) \\ \dot{\mathbf{q}}_{\boldsymbol{\phi}_\mathbf{x}}(t) \\ \dot{\mathbf{q}}_{\boldsymbol{\phi}_\mathbf{y}}(t) \end{Bmatrix}$$
$$+ \begin{bmatrix} \mathbf{K}^{33}_{\mathbf{LS}} + \mathbf{K}^{33}_{\mathbf{NLS}}(\mathbf{q}_{\mathbf{w}}(t)) + \mathbf{F}^{33}_{steady} & \mathbf{K}^{34}_{\mathbf{L}} & \mathbf{K}^{35}_{\mathbf{L}} \\ & \mathbf{K}^{44}_{\mathbf{L}} & \mathbf{K}^{45}_{\mathbf{L}} \\ sym & & \mathbf{K}^{55}_{\mathbf{L}} \end{bmatrix} \begin{Bmatrix} \mathbf{q}_{\mathbf{w}}(t) \\ \mathbf{q}_{\boldsymbol{\phi}_\mathbf{x}}(t) \\ \mathbf{q}_{\boldsymbol{\phi}_\mathbf{y}}(t) \end{Bmatrix} = \begin{Bmatrix} \mathbf{0} \\ \mathbf{0} \\ \mathbf{0} \end{Bmatrix} \quad [7]$$

Linear term $\mathbf{K}^{33}_{\mathbf{LS}}$ and non-linear term $\mathbf{K}^{33}_{\mathbf{NLS}}$ can be found for example in Ref. [31]. This technique reduces the number of DOFs, but tends to increase the bandwidth of the stiffness matrix. The in-plane displacements are still taken into account, just the in-plane inertia is neglected. In this particular study, the set of equations of motion has 3×72=147 DOFs.

2.3 Reduced-Order Model using Modal Summation Method (ROM2)

In the modal summation method employed here, the vibration is assumed to be given by a superposition of selected modes of the system, in the absence of airflow. Structural normal mode shapes are given by the eigenvectors of the linear problem extracted from Equation [4]. Considering a reduced modal matrix composed of m normal modes, the generalized displacements $\mathbf{q}$ can be related to modal displacements $\mathbf{q_m}$ by

$$\mathbf{q}(t) = \boldsymbol{\Phi}\mathbf{q_m}(t). \quad [8]$$

Pre-multiplying the full-order system of Equation [4] by the transpose of the modal matrix, $\boldsymbol{\Phi}^{\boldsymbol{T}}$ and substituting Equation [8] in it, gives m modal equations of motion as following

$$\bar{\mathbf{M}}\ddot{\mathbf{q}}_{\mathbf{m}}(t) + \mathbf{F}_{unsteady}\dot{\mathbf{q}}_{\mathbf{m}}(t) + \left(\bar{\mathbf{K}}_{\mathbf{L}} + \bar{\mathbf{K}}_{\mathbf{NL}} + \bar{\mathbf{F}}_{steady}\right)\mathbf{q}_{\mathbf{m}}(t) = \mathbf{0} \quad [9]$$

where the modal mass matrix $\bar{\mathbf{M}}$ and the linear stiffness matrix $\bar{\mathbf{K}}_{\mathbf{L}}$ are diagonal, but the modal non-linear stiffness matrix $\bar{\mathbf{K}}_{\mathbf{NL}}$ and the modal aerodynamics matrices $\mathbf{F}_{unsteady}$ and $\mathbf{F}_{steady}$ are

not. Naturally, ROM2 has *m* DOFs.

2.4 Reduced-Order Model by Static Condensation and Modal Summation Method (ROM3)

Here, modal summation method is applied on an initially statically condensed model or ROM1. Normal modes are calculated from an already statically condensed linear problem, where airflow velocity is equal to zero. The rest of the procedure is as explained in the previous section. The number of DOFs is again equal to the number of normal modes used.

3. EVALUATION OF THE DEVELOPED MODELS

In the beginning of this section, nonlinear flutter of a simple plate by FOM system is validated against the results published in the literature. Then, amplitudes of nonlinear flutter LCOs by either FOM and associated ROMs are compared. This comparison gives us a criterion to choose an appropriate ROM considering cost of computation and accuracy of results. At the end, the selected ROM will be examined against the number of modes used in its modal reduction method.

3.1 Validation of FOM

For this validation, a comparison between the LCO amplitudes, of an isotropic simply-supported (with immovable edges) square plate, by the current FOM (with 245 DOFs) and by a ROM (with 6 aeroelastic modes by Guo and Mei [2]) is carried out in Figure 2. Based on classical plate theory, Ref. [2] used a ROM with both static condensation and transformation to modal coordinates (aeroelastic). The critical flutter pressure given in [2] and the one by the current method are respectively, λ=512 and λ =514. The small difference between two flutter pressures can be due to the facts that neither the structural theories (TSDT vs. CPT) nor the orders of the systems (FOM with 245 DOFs vs. ROM with 6 DOFs) are equal. This comparison on the nonlinear flutter verifies the correctness and exactness of the present FOM.

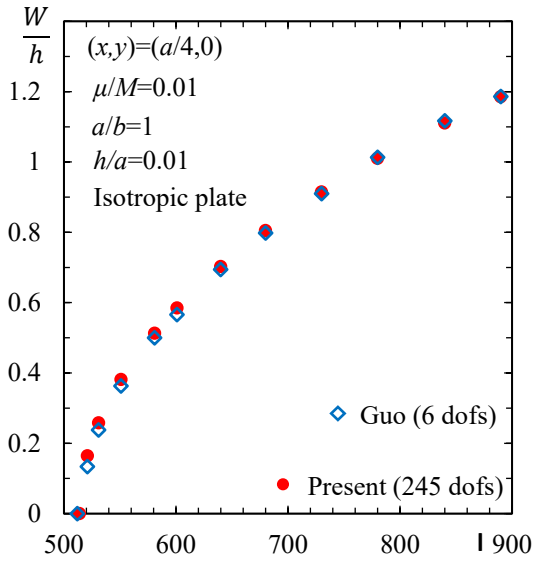

Figure 2. Comparison of LCO amplitudes between the present FOM and the ROM from Guo and Mei [2].

3.2 Comparison Between FOM and Its Associated ROMS

In this comparison study, amplitudes of the nonlinear flutter of a 12-layer VSCL laminate with fiber configurations $[45°+\langle T_0,T_1\rangle,\text{-}45°\text{-}\langle T_0,T_1\rangle,\langle T_0,T_1\rangle,\text{-}\langle T_0,T_1\rangle,90°+\langle T_0,T_1\rangle,\text{-}90°\text{-}\langle T_0,T_1\rangle]_{sym}$, where $\langle T_0,T_1\rangle=\langle 0°,45°\rangle$, are calculated based on developed FOM and ROMs. The mechanical properties of the studied laminate are as follows: E_1 = 126:3 GPa and E_2 = 8:765 GPa, G_{12} = G13 = 4:92 GPa and G_{23} = 3:35 GPa, $\nu_{12} = 0.27$, and $\rho = 1580$ Kg$/m^3$ [31]. Thickness ratio is h/a=0.01 and μ/M is fixed at 0.01. The plate is square, a/b=1, and all the plies have equal thickness. The plate is a cantilever laminate with the edge y=-b/2 clamped and the results are calculated at (x,y)=(0, b/2).

FOM (with 245 physical DOFs), ROM1 (with 147 physical DOFs), ROM2 (with 20 DOFs due to the first 20 normal modes of FOM), and ROM3 (again with 20 DOFs, but now using the first 20 normal modes of ROM1) are evaluated in this comparison. The relative errors, given in the following comparison, measure the accuracy of the ROM approximations taking FOM results as reference.

Table 1. Comparison of LCO amplitudes W/h, by FOM and associated ROMs, of the VSCL against different aerodynamic pressures.

Model	**(DOF)**	λ									
		11.72	11.73	11.75	11.79	11.82	11.87	11.93	11.99	12.07	12.15
FOM	245	0.000	0.152	0.306	0.456	0.569	0.703	0.853	0.963	1.105	1.225
ROM1	147	0.085	0.151	0.305	0.456	0.568	0.701	0.852	0.961	1.103	1.223
Error %		-	-0.2	-0.2	-0.2	-0.2	-0.2	-0.2	-0.2	-0.2	-0.2
ROM2	20	0.004	0.013	0.027	0.040	0.050	0.061	0.075	0.084	0.096	0.106
Error %		-	-91.5	-91.2	-91.2	-91.2	-91.2	-91.3	-91.3	-91.3	-91.3
ROM3	20	0.005	0.066	0.304	0.455	0.567	0.701	0.851	0.961	1.103	1.222
Error %		-	-56.3	-0.6	-0.4	-0.3	-0.3	-0.2	-0.2	-0.2	-0.2

Based on the comparison performed in Table 1, the best approximations to the results of FOM are those obtained using ROM1. Between ROMs with 20 DOFs, ROM3 predicts more exact results than ROM2. The error between the amplitudes calculated by ROMs and FOM, in the largest deflection ratio, is 0.2 %, 91.3 % and 0.2 % for ROM1, ROM2, and ROM3, respectively. One may expect these approximations since, in this analysis, lower frequencies (so their normal modes) are associated with out-of-plane deflection and higher frequencies (so their normal modes) are connected with in-plane displacements. In the case of ROM2, the first 20 modes do not necessarily include in-plane modes (in-plane and out-of-plane modes are uncoupled). But in the case of ROM3, coupling between in-plane and out-of-plane modes exists and consequently

the first 20 modes include membrane effects. This explains the fact that in this case, ROM3 gives a better approximation than ROM2. It is obvious that ROM2 leads to the worst approximation. It should be noted that all ROMs predict the (critical) linear flutter at lower dynamic pressure and underestimate the deflection results in nonlinear flutter, in comparison with FOM. Naturally, a ROM2 with all normal modes included predicts results equal to its associated FOM. In case of ROM3, this model with all modes predicts results equal to ROM1.

Regarding the expense of computation seen during calculation of Table 1, FOM had the highest computational cost; ROM1 had a computational cost just slightly lower than the one of FOM; ROM2 and ROM3 had the lowest computational cost. Based on the comparison in this table, ROM3 can be considered as the fastest model with acceptable deflection results, among the three methods to reduce the order here considered.

3.3 Convergence of ROM3

Considering selection of ROM3 from the previous sub-section, based on its cost of computation and its exactness, the mentioned model is investigated against the number of modes (DOFs), here in Table 2. This table demonstrates that LCO amplitudes in the nonlinear flutter of the VSCL predicted by ROM3 with 14 modes (DOFs) are less than 1 % away from those calculated by FOM.

Table 2. LCO amplitudes W/h of the VSCL against different aerodynamic pressures, calculated using FOM and predicted by ROM3 with different number of modes.

Model	**DOF**	λ									
		11.72	11.73	11.75	11.79	11.82	11.87	11.93	11.99	12.07	12.15
FOM	245	0.000	0.152	0.306	0.456	0.569	0.703	0.853	0.963	1.105	1.225
ROM3	4	0.000	0.000	0.000	0.000	0.000	0.000	0.000	0.769	0.928	1.057
Error %		-	-100.0	-100.0	-100.0	-100.0	-100.0	-100.0	-20.1	-16.0	-13.7
ROM3	6	0.000	0.000	0.000	0.384	0.517	0.666	0.828	0.944	1.093	1.218
Error %		-	-100.0	-100.0	-15.8	-9.1	-5.3	-3.0	-2.0	-1.1	-0.6
ROM3	8	0.002	0.008	0.288	0.444	0.559	0.694	0.846	0.957	1.099	1.219
Error %		-	-94.9	-5.8	-2.6	-1.7	-1.2	-0.8	-0.7	-0.5	-0.5
ROM3	10	0.000	0.000	0.226	0.426	0.544	0.682	0.835	0.947	1.090	1.210
Error %		-	-99.9	-26.2	-6.7	-4.4	-3.0	-2.1	-1.7	-1.4	-1.2
ROM3	12	0.003	0.024	0.296	0.449	0.563	0.697	0.848	0.958	1.100	1.219
Error %		-	-83.9	-3.2	-1.6	-1.1	-0.8	-0.7	-0.6	-0.5	-0.5
ROM3	14	0.005	0.067	0.304	0.455	0.567	0.700	0.851	0.961	1.103	1.222
Error %		-	-55.5	-0.6	-0.4	-0.4	-0.3	-0.3	-0.3	-0.2	-0.3
ROM3	16	0.005	0.067	0.304	0.455	0.567	0.701	0.851	0.961	1.103	1.222
Error %		-	-55.9	-0.6	-0.4	-0.3	-0.3	-0.2	-0.2	-0.2	-0.2
ROM3	18	0.005	0.068	0.304	0.455	0.567	0.701	0.851	0.961	1.103	1.222
Error %		-	-55.0	-0.6	-0.3	-0.3	-0.2	-0.2	-0.2	-0.2	-0.2

4. RESULTS

Based on the convergence and comparison demonstrated in this paper, ROM3 with 14 modes (DOFs) is employed in the analyses below. Table 3 and Figure 3 present the critical flutter pressure and LCO amplitudes, respectively, of VSCL plates where T_0 and T_1 are changing. The VSCL has fiber configuration like [45°+$\langle T_0,T_1\rangle$, -45°-$\langle T_0,T_1\rangle$,$\langle T_0,T_1\rangle$,-$\langle T_0,T_1\rangle$,90°+$\langle T_0,T_1\rangle$,-90°-$\langle T_0,T_1\rangle$]$_{sym}$ and mechanical properties as defined in section 3.2. It is seen that increasing the fiber angle at the right edge, T_1, from 0° to 45° increases the critical flutter pressure by around 1.2 times. Contrary to the right edge, increasing the fiber angle at the left edge, T_0, from 0° to 45° decreases the critical flutter pressure by around 0.7 times.

Figure 3 displays amplitudes of LCOs against relative aerodynamic pressure, where the nonlinear flutter of the VSCL plates are analyzed. The relative aerodynamic pressure is calculated as λ/λ_l, where λ_l is the critical aerodynamic pressure. Based on this figure, hardening effect happens in all the VSCLs studied. By increasing the fiber angle at the left edge, T_0, hardening effect intensifies and, therefore, a VSCL with larger T_0 experiences less deflection. Figure 3b implies that the hardening effect does not change meaningfully with the fiber angle at the right edge, T_1, especially when it is less than 30°. If the fiber angle at the right edge, T_1, increases to 45°, hardening decreases and the VSCL plate experiences less LCO amplitudes.

Table 3. Critical flutter pressure of VSCL plates against fiber angle at the left edge T_0 and at the right edge T_1.

T_0=0°	T_1				
	0°	10°	20°	30°	45°
λ	1304.9	1339.0	1392.1	1462.9	1588.2
T_1=0°	T_0				
	0°	10°	20°	30°	45°
λ	1304.9	1283.2	1206.2	1091.8	938.6

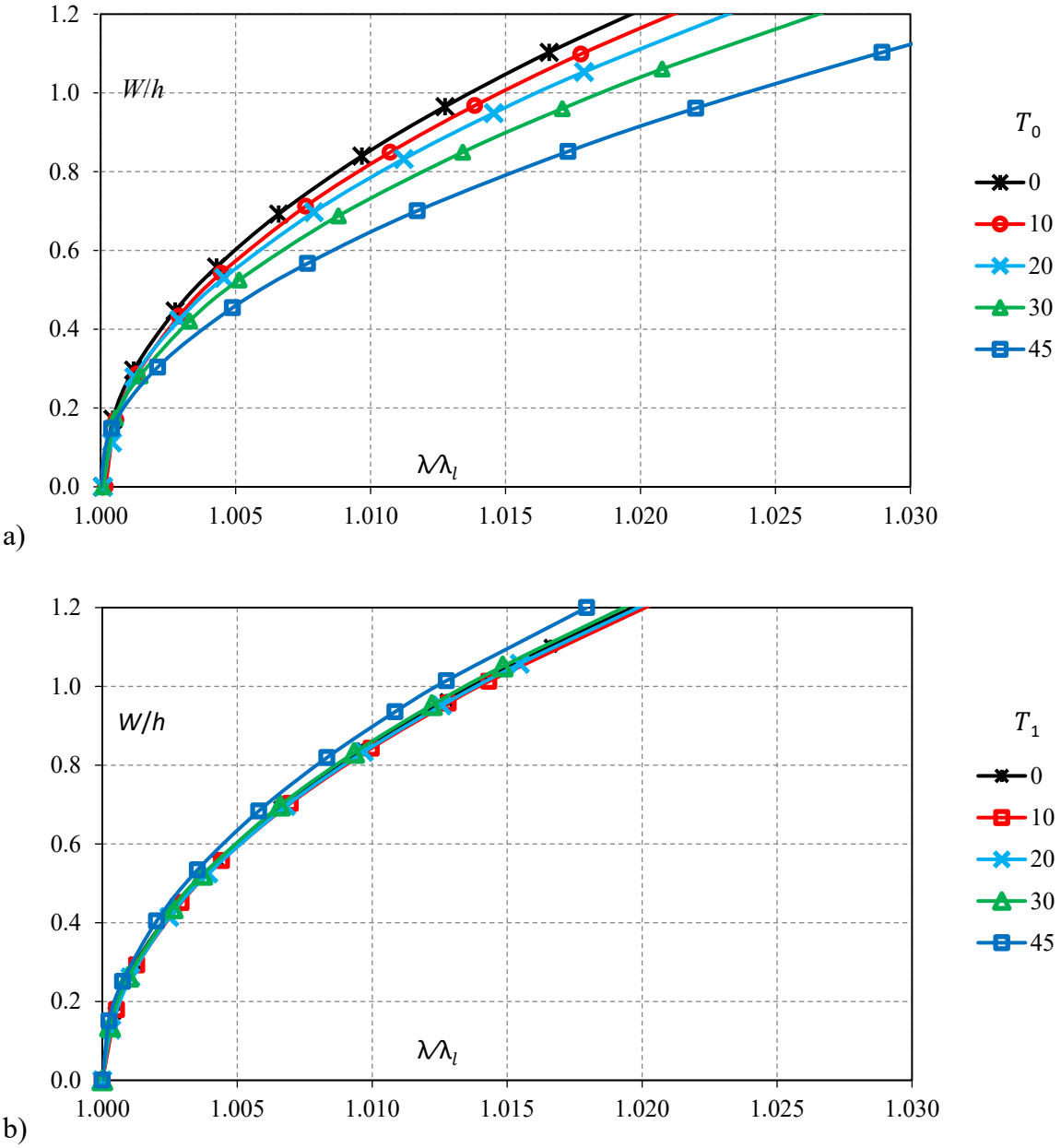

Figure 3. LCO amplitudes W/h against different aerodynamic pressures λ, for VSCLs with various fiber angle parameters; a) change of T_0 ($T_1 = 0°$), and b) change of T_1 ($T_0 = 0°$).

5. CONCLUSIONS

Rectangular composite laminates with curvilinear fiber paths, defined as one type of VSCL plates, were studied in this paper. The curvilinear fiber orientation changed linearly from the left

edge to the right one. Nonlinear flutter of the studied VSCLs was investigated using full-order and reduced-order models. Full-order model obtained based on a third-order shear deformation theory coupled with *p*-version finite element method. Reduced-order models calculated on the basis of static condensation and modal summation techniques applied on the full-order model. It was shown that reduced-order model using both static condensation and modal summation method with at least 14 structural modes can predict the deflection results with an approximation less than 1 % with respect to the results by the full-order model. Finally, linear (critical) flutter pressure as well as LCO amplitudes of self-oscillation in nonlinear flutter of VSCL plates were analyzed against different fiber angle parameters. Also, it was shown that fiber angles in left or right edges of the plate have different effect on the aerodynamic properties of VSCL plates.

ACKNOWLEDGMENTS

The authors gratefully acknowledge the funding of Project NORTE-01-0145-FEDER-000022 - SciTech - Science and Technology for Competitive and Sustainable Industries, cofinanced by Prog. Operacional Reg. do Norte (NORTE2020), through Fundo Europeu de Des. Regional (FEDER).

6. REFERENCES

1. Thompson, J. M. T., and Stewart, H. B., *Nonlinear Dynamics and Chaos*, John Wiley & Sons, 2002.
2. Guo, X., and Mei, C., "Using Aeroelastic Modes for Nonlinear Panel Flutter at Arbitrary Supersonic Yawed Angle," AIAA Journal, Vol. 41, No. 2, 2003, pp. 272–279. doi:10.2514/2.1940
3. Przekop, A., Guo, X., and Rizzi, S. A., "Alternative Modal Basis Selection Procedures for Reduced-Order Nonlinear Random Response Simulation," Journal of Sound and Vibration, Vol. 331, No. 17, 2012, pp. 4005–4024. doi:10.1016/j.jsv.2012.03.034
4. Rizzi, S. A., and Przekop, A., "System Identification-Guided Basis Selection for Reduced-Order Nonlinear Response Analysis," Journal of Sound and Vibration, Vol. 315, No. 3, 2008, pp. 467–485. doi:10.1016/j.jsv.2007.12.031
5. Gai, G., and Timme, S., "Nonlinear Reduced-Order Modelling for Limit-Cycle Oscillation Analysis," Nonlinear Dynamics, Vol. 84, No. 2, 2016, pp. 991–1009. doi:10.1007/s11071-015-2544-9
6. Gang, C., Yingtao, Z., Jian, S., and Yueming, L., "Support-Vector-Machine-Based Reduced-Order Model for Limit Cycle Oscillation Prediction of Nonlinear Aeroelastic System," Mathematical Problems in Engineering, Vol. 2012, 2012. doi:10.1155/2012/152123
7. Gang, C., Yueming, L., and Guirong, Y., "Active Control Law Design for Flutter/LCO Suppression Based on Reduced Order Model Method," Chinese Journal of Aeronautics, Vol. 23, No. 6, 2010, pp. 639–646. doi:10.1016/s1000-9361(09)60265-x
8. Balajewicz, M., and Dowell, E., "Reduced-Order Modeling of Flutter and Limit-Cycle Oscillations using the Sparse Volterra Series," Journal of Aircraft, Vol. 49, No. 6, 2012, pp. 1803–1812. doi:10.2514/1.c031637

9. Zhang, W., Wang, B., and Ye, Z., “High Efficient Numerical Method for Limit Cycle Flutter Analysis Based on Nonlinear Aerodynamic Reduced-Order-Model,” 51st AIAA, ASME, ASCE, AHS, ASC Structures, Structural Dynamics and Material Conference, Orlando, Florida, 2010. doi:10.2514/6.2010-2723
10. Akhavan, H., and Ribeiro, P., “Natural Modes of Vibration of Variable Stiffness Composite Laminates with Curvilinear Fibers,” Composite Structures, Vol. 93, No. 11, 2011, pp. 3040–3047. doi:10.1016/j.compstruct.2011.04.027
11. Akhavan, H., Ribeiro, P., and De Moura, M. F. S. F., “Large Deflection and Stresses in Variable Stiffness Composite Laminates with Curvilinear Fibres,” International Journal of Mechanical Sciences, Vol. 73, 2013, pp. 14–26. doi:10.1016/j.ijmecsci.2013.03.013
12. Akhavan, H., Ribeiro, P., and De Moura, M. F. S. F., “Damage Onset on Tow-Placed Variable Stiffness Composite Laminates,” Composite Structures, Vol. 113, 2014, pp. 419–428. doi:10.1016/j.compstruct.2014.03.038
13. Ribeiro, P., “Non-Linear Free Periodic Vibrations of Variable Stiffness Composite Laminated Plates,” Nonlinear Dynamics, Vol. 70, No. 2, 2012, pp. 1535–1548. doi:10.1007/s11071-012-0554-4
14. Ribeiro, P., “Non-Linear Modes of Vibration of Thin Cylindrical Shells in Composite Laminates with Curvilinear Fibres,” Composite Structures, Vol. 122, 2015, pp. 184–197. doi:10.1016/j.compstruct.2014.11.019
15. Ribeiro, P., and Stoykov, S., “Forced Periodic Vibrations of Cylindrical Shells in Laminated Composites with Curvilinear Fibres,” Composite Structures, Vol. 131, 2015, pp. 462–478. doi:10.1016/j.compstruct.2015.05.050
16. Akhavan, H., and Ribeiro, P., “Geometrically Non-Linear Periodic Forced Vibrations of Imperfect Laminates with Curved Fibres by the Shooting Method,” Composites Part B: Engineering, Vol. 109, No. 15, 2017, pp. 286–296. doi:10.1016/j.compositesb.2016.10.059
17. Akhavan, H., and Ribeiro, P., “Free Geometrically Nonlinear Oscillations of Perfect and Imperfect Laminates with Curved Fibres by the Shooting Method,” Nonlinear Dynamics, Vol. 81, No. 1-2, 2015, pp. 949–965. doi:10.1007/s11071-015-2043-z
18. Akhavan, H., and Ribeiro, P., “Non-Linear Forced Periodic Oscillations of Laminates with Curved Fibres by the Shooting Method,” International Journal of Non-Linear Mechanics, Vol. 76, 2015, pp. 176–189. doi:10.1016/j.ijnonlinmec.2015.06.004
19. Akhavan, H., and Ribeiro, P., “Aeroelasticity of Composite Plates with Curvilinear Fibres in Supersonic Flow,” Composite Structures, Vol. 194, No. 15, 2018, pp. 335–344. doi:10.1016/j.compstruct.2018.03.101
20. Ribeiro P, Akhavan H, Teter A, Warmiński J. A review on the mechanical behaviour of curvilinear fibre composite laminated panels. Journal of Composite Materials. 2014 Sep;48(22):2761-77. DOI: /10.1177/0021998313502066
21. Lukaszewicz, D. H. J. A., Ward, C., and Potter, K. D., “The Engineering Aspects of Automated Prepreg Layup: History, Present and Future,” Composites Part B: Engineering, Vol. 43, No. 3, 2012, pp. 997–1009. doi:10.1016/j.compositesb.2011.12.003

22. Ungwattanapanit, T., and Baier, H., “Postbuckling Analysis and Optimization of Stiffened Fuselage Panels Utilizing Variable-Stiffness Laminates,” Proceedings of 29th Congress of the International Council of the Aeronautical Sciences (ICAS2014), St. Petersburg, Russia, 2014, p. 68.
23. Stanford, B. K., and Jutte, C. V., “Comparison of Curvilinear Stiffeners and Tow Steered Composites for Aeroelastic Tailoring of Aircraft Wings,” Computers & Structures, Vol. 183, 2017, pp. 48–60. doi:10.1016/j.compstruc.2017.01.010
24. Stanford, B. K., Jutte, C. V., and Wu, K. C., “Aeroelastic Benefits of Tow Steering for Composite Plates,” Composite Structures, Vol. 118, 2014, pp. 416–422. doi:10.1016/j.compstruct.2014.08.007
25. Haddadpour, H., and Zamani, Z., “Curvilinear Fiber OptimizationTools for Aeroelastic Design of Composite Wings,” Journal of Fluids and Structures, Vol. 33, 2012, pp. 180–190. doi:10.1016/j.jfluidstructs.2012.05.008
26. Guimarães, T. A. M., Castro, S. G. P., Rade, D. A., and Cesnik, C. E. S., “Panel Flutter Analysis and Optimization of Composite Tow Steered Plates,” 58th AIAA/ASCE/AHS/ASC Structures, Structural Dynamics, and Materials Conference, Grapevine, Texas, 2017, p. 1118. doi:10.2514/6.2017-1118
27. Akhavan, H., and Ribeiro, P., “Reduced-Order Models for Non-Linear Flutter of Composite Laminates with Curvilinear Fibers”, 2018, submitted to AIAA Journal.
28. Vlasov, B. F., “On the Equations of Bending of Plates,” Dokla Ak Nauk Azerbeijanskoi-SSR, Vol. 3, 1957, pp. 955–979
29. Reddy, J. N., Mechanics of Laminated Composite Plates and Shells: Theory and Analysis, CRC Press, 2004. doi:10.1201/b12409
30. Han, W., Petyt, M., and Hsiao, K. M., “An Investigation into Geometrically Nonlinear Analysis of Rectangular Laminated Plates using the Hierarchical Finite Element Method,” Finite Elements in Analysis and Design, Vol. 18, No. 1-3, 1994, pp. 273–288. doi:10.1016/0168-874x(94)90107-4
31. Akhavan, H., “Non-Linear Vibrations of Tow Placed Variable Stiffness Composite Laminates,” Ph.D. thesis, University of Porto, 2015.
32. Dowell, E. H., Clark, R., Cox, D., Curtiss, H. C., Edwards, J. W., Hall, K. C., Peters, D. A., Scanlan, R., Simiu, E., Sisto, F., et al., A Modern Course in Aeroelasticity, Kluwer Academic Publishers, Dordrecht, 2004.
33. Meirovitch, L., Computational Methods in Structural Dynamics, Springer Science & Business Media, 1980.